

from a combination of a classical solvent effect (equilibrium solvation of the transition state) and various PNS effects arising from nonequilibrium solvation of different parts of the transition state. For the comparison between water and Me<sub>2</sub>SO, the PNS analysis suggests that the equilibrium and nonequilibrium solvation effects of the transition state contribute approximately equally to the large overall change in  $k_0$  ( $\Delta G_0^*$ (obsd)). If  $|m - z_{TS}|$  is assumed to be 0.25, which seems to be a reasonable value, the Kurz analysis leads to a similar breakdown into equilibrium and nonequilibrium solvation effects.

For the change from Me<sub>2</sub>SO to MeCN, the PNS analysis suggests that the observed increase in  $k_0$  (decrease in  $\Delta G_0^*$ (obsd)) is in large measure an equilibrium solvation effect, although there is a small contribution by a nonequilibrium solvation effect. The Kurz model also predicts an increase in  $k_0$  (decrease in  $\Delta G_0^*$ (obsd)) from an equilibrium solvation effect but a rather small one. On the other hand, assuming  $|m - z_{TS}| = 0.25$  as above, the Kurz model calls for a substantial decrease in  $k_0$  (increase in  $\Delta G_0^*$ (obsd)) by nonequilibrium solvation, which completely offsets

(or even overcompensates) the equilibrium solvation effect in contradiction with the experimental results.

**Acknowledgment.** This research was supported by Grant CHE-8921739 from the National Science Foundation.

**Registry No.** (3-Nitrophenyl)nitromethane, 34063-52-0; (4-nitrophenyl)nitromethane, 1610-26-0; (3,5-dinitrophenyl)nitromethane, 70136-12-8; tetraethylammonium benzoate, 16909-22-1; tetraethylammonium 3-bromobenzoate, 68570-54-7; tetraethylammonium 4-bromobenzoate, 137570-74-2; benzoate, 766-76-7; 3-bromobenzoate, 16887-61-9; 4-bromobenzoate, 2906-29-8; (3-nitrophenyl)nitromethyl anion, 66291-20-1; (4-nitrophenyl)nitromethyl anion, 66291-19-8; 3,5-dinitrobenzyl bromide, 137570-75-3; 3,5-dinitrobenzyl alcohol, 71022-43-0.

**Supplementary Material Available:** Tables (S1-S8) of kinetic and equilibrium data for benzoic acid, the phenylnitromethanes, and their corresponding anions (8 pages). Ordering information is given on any current masthead page.

## Structure and Thermodynamic and Kinetic Properties of Eosin-Bipyridinium Complexes

Itamar Willner,\* Yoav Eichen, Mordecai Rabinovitz, Roy Hoffman, and Shmuel Cohen

Contribution from the Institute of Chemistry, The Hebrew University of Jerusalem, Jerusalem 91904, Israel. Received July 12, 1991

**Abstract:** Eosin, Eo<sup>2-</sup>, and *N,N'*-dimethyl-4,4'-bipyridinium, MV<sup>2+</sup>, form a crystalline 1:1 complex [Eo<sup>2-</sup>-MV<sup>2+</sup>]. With *N,N'*-dibenzyl-4,4'-bipyridinium, BV<sup>2+</sup>, the dye Eo<sup>2-</sup> forms a crystalline complex where one BV<sup>2+</sup> unit is intercalated between two Eo<sup>2-</sup> units and the second BV<sup>2+</sup> unit is positioned outside this sandwich structure [Eo<sup>2-</sup>-BV<sup>2+</sup>-Eo<sup>2-</sup>;BV<sup>2+</sup>]. Electrostatic, charge-transfer, and  $\pi$  interactions stabilize these intermolecular assemblies. In solution, Eo<sup>2-</sup> and MV<sup>2+</sup> initially form the 1:1 intermolecular structure [Eo<sup>2-</sup>-MV<sup>2+</sup>]. The latter complex is transformed to the thermodynamically stable complex structure [Eo<sup>2-</sup>-MV<sup>2+</sup>-Eo<sup>2-</sup>;MV<sup>2+</sup>] (in DMF,  $k = 57.3 \text{ M}^{-1} \text{ s}^{-1}$  at 331 K and  $E_a = 25.3 \pm 0.5 \text{ kcal mol}^{-1}$ ). The 1:1 complex [Eo<sup>2-</sup>-MV<sup>2+</sup>] shows thermal population of the charge-transfer band.

Attractive interactions between  $\pi$ -systems control the formation of diverse molecular complexes. Stabilization of the double helical structure of DNA<sup>1</sup>, intercalation of drugs into DNA,<sup>2,3</sup> stacking of aromatic molecules in the crystal structure,<sup>4</sup> formation of host-guest complexes,<sup>5,6</sup> and aggregation of organic dyes<sup>7</sup> or porphyrins<sup>8</sup> originate from intermolecular  $\pi$ - $\pi$  interactions. Theoretical studies have outlined the significance of  $\pi$ -interactions in controlling orientational effects and the structure of  $\pi$ -stacked

systems.<sup>9</sup> Electron donor-acceptor interactions provide another route for the stabilization of molecular complexes.<sup>10</sup> Selective molecular complexation in biological systems<sup>11,12</sup> and formation of stable host-guest assemblies<sup>13,14</sup> have been attributed to stabilizing electron donor-acceptor interactions. The interactions in electron donor-acceptor complexes might originate from electrostatic interactions, polarization interactions, charge-transfer interactions, and dispersion energy. It has been emphasized<sup>9</sup> that  $\pi$ -interactions and electron donor-acceptor interactions are two different mechanisms leading to the stabilization of molecular complexes. While  $\pi$ - $\pi$  interactions are controlled by the intermolecular contact of the components in the complex, electron donor-acceptor interactions are influenced by the oxidation and reduction potentials of the components. Nevertheless, the two modes can act cooperatively in the selective stabilization of defined molecular complexes.<sup>15</sup>

Xanthene dyes exhibit photophysical properties that allow their application as photosensitizers in photosynthetic systems.<sup>16-18</sup>

(1) Saenger, W. *Principles of Nucleic Acid Structure*; Springer Verlag: New York, 1984; pp 132-140.

(2) Wakelin, L. P. G. *Med. Res. Rev.* **1986**, *6*, 275.

(3) Wang, A. H.-J.; Ughetto, G.; Quigley, G. J.; Rich, A. *Biochemistry* **1987**, *26*, 1152.

(4) (a) Foster, L. *Organic Charge-Transfer Complexes*; Academic Press: New York, 1969; Chapter 8. (b) *Organic Solid-State Chemistry*; Desiraju, G. R., Ed.; Elsevier: Amsterdam, 1987. (c) Desiraju, G. R.; Gavezzotti, A. *J. Chem. Soc., Chem. Commun.* **1989**, 621.

(5) (a) Askew, B.; Ballester, P.; Buhr, C.; Jeong, K. S.; Jones, S.; Parris, K.; Williams, K.; Rebek, J., Jr. *J. Am. Chem. Soc.* **1989**, *111*, 1082. (b) Jazwinski, J.; Blacker, A. J.; Lehn, J.-M.; Cesario, M.; Guilhem, J.; Pascard, C. *Tetrahedron Lett.* **1987**, *28*, 6057. (c) Orthaland, J.-Y.; Slawin, A. M. Z.; Spencer, N.; Stoddart, J. F.; Williams, D. J. *Angew. Chem., Int. Ed. Engl.* **1989**, 1394.

(6) (a) Zimmerman, S. C.; Van Zyl, C. M.; Hamilton, G. S. *J. Am. Chem. Soc.* **1989**, *111*, 1373. (b) Zimmerman, S. C.; Mrksich, M.; Baloga, M. *J. Am. Chem. Soc.* **1989**, *111*, 8528. (c) Ferguson, S. B.; Diedrich, F. *Angew. Chem., Int. Ed. Engl.* **1986**, *25*, 1127. (d) Sheridan, R. E.; Whitlock, H. W. *J. Am. Chem. Soc.* **1988**, *110*, 4071. (e) Schneider, H.-J.; Blatter, T.; Simova, S.; Thesis, I. *J. Chem. Soc., Chem. Commun.* **1989**, 580.

(7) Valdes-Aguillera, D.; Neckers, D. C. *Acc. Chem. Res.* **1989**, *22*, 171 and references cited therein.

(8) (a) Abraham, R. J.; Eivazi, F.; Pearson, H.; Smith, K. M. *J. Chem. Soc., Chem. Commun.* **1976**, 699. (b) Scheidt, W. R.; Lee, Y. J. *Structure and Bonding*; Springer-Verlag: Berlin, 1987; Vol. 64.

(9) Hunter, C. A.; Sanders, J. K. M. *J. Am. Chem. Soc.* **1990**, *112*, 5525.

(10) (a) Hanna, M. W.; Lippert, J. L. In *Molecular Complexes*; Foster, R., Ed.; Elek Science: London, 1973; Vol. 1. (b) Bender, C. J. *Chem. Soc. Rev.* **1986**, *15*, 475.

(11) Pullman, B.; Pullman, A. *Quantum Biochemistry*; Wiley-Interscience: New York, 1963.

(12) Clavrie, P. In *Intermolecular Interactions: From Diatomics to Biopolymers*; Pullman, B., Ed.; Wiley: Chichester, England, 1978, p 69-306.

(13) (a) Rebek, J., Jr.; Nemeth, D. *J. Am. Chem. Soc.* **1985**, *107*, 6738.

(b) Pirkle, W. H.; Pochaspy, J. C. *J. Am. Chem. Soc.* **1987**, *109*, 5975.

(14) Rubin, Y.; Dick, R.; Diedrich, F.; Georgiadis, T. M. *J. Org. Chem.* **1986**, *51*, 3270.

(15) Diedrich, F. *Angew. Chem., Int. Ed. Engl.* **1988**, *27*, 362.

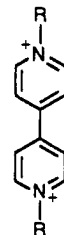
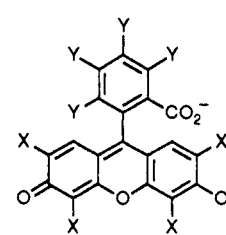
Table I. Crystallographic Data for Xanthene Dye-Bipyridinium Complexes

	[Eo <sup>2-</sup> -MV <sup>2+</sup> ]	[Eo <sup>2-</sup> -BV <sup>2+</sup> ]	[Phl <sup>2-</sup> -BV <sup>2+</sup> ]
formula	C <sub>20</sub> H <sub>6</sub> O <sub>5</sub> Br <sub>4</sub> ·C <sub>12</sub> H <sub>14</sub> N <sub>2</sub> ·13H <sub>2</sub> O	C <sub>20</sub> H <sub>6</sub> O <sub>5</sub> Br <sub>4</sub> ·C <sub>24</sub> H <sub>22</sub> N <sub>2</sub> ·2H <sub>2</sub> O	C <sub>20</sub> H <sub>6</sub> O <sub>5</sub> Br <sub>4</sub> ·Cl <sub>4</sub> ·C <sub>24</sub> H <sub>22</sub> N <sub>2</sub> ·3CH <sub>3</sub> OH
MW	1078.3	1026.4	1218.2
space group	P $\bar{1}$	P $\bar{1}$	P $\bar{1}$
a, Å	12.103 (3)	13.665 (4)	13.654 (6)
b, Å	15.192 (6)	13.771 (4)	14.530 (7)
c, Å	11.555 (4)	12.230 (3)	12.620 (4)
$\alpha$ , deg	91.88 (6)	92.00 (3)	104.99 (5)
$\beta$ , deg	94.80 (5)	111.13 (3)	103.71 (4)
$\gamma$ , deg	97.61 (4)	81.91 (4)	82.7 (5)
V, Å <sup>3</sup>	2096.4 (9)	2125.0 (9)	2344 (1)
Z	2	2	2
$\rho_{\text{calcd}}$ , g cm <sup>-3</sup>	1.71	1.60	1.73
$\mu(\text{MoK}\alpha)$ , cm <sup>-1</sup>	38.09	37.39	36.11
no. of unique reflections	7101	5723	6385
no. of reflections with $I > 3\sigma_I$	4059	3166	4508
R	0.065	0.083	0.065
R <sub>w</sub>	0.083	0.126	0.089
w <sup>-1</sup>	$\sigma_F^2 + 0.000151F^2$	$\sigma_F^2 + 0.008959F^2$	$\sigma_F^2 + 0.006774F^2$

Photosensitized electron-transfer reactions and subsequent hydrogen evolution have been reported using *N,N'*-dimethyl-4,4'-bipyridinium, methyl viologen, MV<sup>2+</sup>, as the primary electron acceptor, various xanthene dyes, i.e., eosin or rose bengal, and Pt as the heterogeneous catalyst.<sup>16,17</sup> Photosensitization of semiconductor colloids, i.e., TiO<sub>2</sub>, by xanthene dyes provides another route for the application of these dyes in photocatalytic assemblies.<sup>18</sup> Nevertheless, the application of xanthene dyes in photosensitized electron-transfer reactions is often accompanied by the formation of ground-state dye-electron acceptor complexes.<sup>19,20</sup> For example, xanthene dye forms intermolecular complexes with bipyridinium salts such as MV<sup>2+</sup>. These complexes act destructively toward the separation of electron-transfer products, and microheterogeneous systems capable of separating these complexes and controlling the electron-transfer process have been developed.<sup>21</sup> Till now, the formation of these complexes has been followed by absorption spectroscopy, but no insight into the structural features or reactivity of these complexes is available.

Molecular complexes that include *N,N'*-dialkyl-4,4'-bipyridinium compounds as electron acceptors and various electron donors have been structurally characterized<sup>22</sup> and their photo-physical properties have been determined.<sup>23</sup> Here we wish to describe a detailed characterization of the crystal and solution structures of the complexes formed between eosin (**1**) and the electron acceptors *N,N'*-dimethyl-4,4'-bipyridinium, MV<sup>2+</sup> (**2**), and *N,N'*-dibenzyl-4,4'-bipyridinium, BV<sup>2+</sup> (**3**). The crystal structure of phloxine (**4**) and BV<sup>2+</sup> (**3**) complex is also provided. We highlight the structural features of eosin, Eo<sup>2-</sup> (**1**), and MV<sup>2+</sup> (**2**) complexes in solutions. We describe the initial formation of a 1:1 assembly, Eo<sup>2-</sup>-MV<sup>2+</sup>, that is transformed to a thermody-

namically stable complex that includes the MV<sup>2+</sup> unit intercalated between two eosin components [Eo<sup>2-</sup>-MV<sup>2+</sup>-Eo<sup>2-</sup>;MV<sup>2+</sup>]. The former complex, Eo<sup>2-</sup>-MV<sup>2+</sup>, shows thermal population<sup>22b,24</sup> of the charge-transfer level. We demonstrate that  $\pi$ - $\pi$  intermolecular interactions and electrostatic interactions play important roles in shaping the structure of xanthene dye-bipyridinium complexes.

2 (MV<sup>2+</sup>), R = CH<sub>3</sub>3 (BV<sup>2+</sup>), R = CH<sub>2</sub>Ph1 (Eo<sup>2-</sup>), X = Br, Y = H4 (Phl<sup>2-</sup>), X = Br, Y = Cl

## Experimental Section

**Materials.** Eosin Y disodium salt, Eo<sup>2-</sup> (**1**) (BDH), phloxine B disodium salt, Phl<sup>2-</sup> (**4**) (Aldrich), *N,N'*-dimethyl-4,4'-bipyridinium dichloride, MV<sup>2+</sup> (**2**) (Aldrich), and *N,N'*-dibenzyl-4,4'-bipyridinium dichloride, BV<sup>2+</sup> (**3**), were used without further purification.

**Instruments.** Absorption spectra were recorded on an Uvikon 860 (Kontron) spectrophotometer equipped with a thermostatic cell. NMR spectra were recorded on an AMX 400 spectrometer (Bruker). ESR spectra were recorded on an ESP 380 spectrometer (Bruker).

**X-ray Crystal Structure Analysis.** Data were measured on a PW1100/20 (Philips) four-circle computer-controlled diffractometer. Mo K $\alpha$  ( $\lambda = 0.71069$  Å) radiation with a graphite crystal monochromator in the incident beam was used. The unit cell dimensions were obtained by a least-squares fit of 20 (for the eosin-MV<sup>2+</sup> [Eo<sup>2-</sup>-MV<sup>2+</sup>] complex) or 24 (for the eosin-BV<sup>2+</sup> [Eo<sup>2-</sup>-BV<sup>2+</sup>-Eo<sup>2-</sup>;BV<sup>2+</sup>] and phloxine-BV<sup>2+</sup> [Phl<sup>2-</sup>-BV<sup>2+</sup>-Phl<sup>2-</sup>;BV<sup>2+</sup>] complexes) centered reflections in the range of  $10^\circ \leq \theta \leq 14^\circ$ . Intensity data were collected using the  $\omega$ - $2\theta$  technique to a maximum  $2\theta$  of  $50^\circ$ ,  $46^\circ$ , and  $46^\circ$  (for [Eo<sup>2-</sup>-MV<sup>2+</sup>], [Eo<sup>2-</sup>-BV<sup>2+</sup>-Eo<sup>2-</sup>;BV<sup>2+</sup>], and [Phl<sup>2-</sup>-BV<sup>2+</sup>-Phl<sup>2-</sup>;BV<sup>2+</sup>] respectively). The scan width,  $\Delta\omega$ , for each reflection was  $1.00 + 0.35 \tan \theta$  with a scan speed of 3.0 deg/min. Background measurements were made for a total of 20 s at both limits of each scan. Three standard reflections were monitored every 60 min. No variations in intensities were found. Intensities were corrected for Lorentz, polarization, and absorption effects. All non-hydrogen atoms were found by using the results of the SHELXS-86 direct-method analysis (Sheldrick G. M. *Crystallographic Computing 3*; Oxford University Press, Oxford, 1985; pp 175-189). After several cycles of refinements, the positions of the hydrogen atoms were calculated and added with a constant isotropic temperature factor of  $0.08 \text{ \AA}^2$  to the refinement process.<sup>25</sup> Refinement proceeded to convergence by mini-

(16) (a) Usui, Y.; Sasaki, Y.; Ishii, Y.; Tokumaru, K. *Bull. Chem. Soc. Jpn.* **1988**, *61*, 3335. (b) Hashimoto, K.; Kawai, T.; Sakata, T. *Chem. Lett.* **1983**, 709.

(17) (a) Mau, A. W.-H.; Johansen, O.; Sasse, W. H. F. *Photochem. Photobiol.* **1985**, *41*, 503. (b) Ghigginio, K. P.; Brown, J. M.; Launikonis, A.; Mau, A. W.-H.; Sasse, W. H. F. *Aust. J. Chem.* **1988**, *41*, 9.

(18) (a) Kamat, P. V.; Fox, M. A. *J. Phys. Chem.* **1984**, *88*, 2297. (b) Moser, J.; Grätzel, M. *J. Am. Chem. Soc.* **1984**, *106*, 6557. (c) Shimidzu, T.; Iyoda, T.; Kolde, Y. *J. Am. Chem. Soc.* **1985**, *107*, 35.

(19) (a) Okura, I.; Kusunoki, S.; Aono, S. *Inorg. Chim. Acta* **1983**, *77*, L99. (b) Sato, T.; Ogawa, T.; Kano, K. *J. Phys. Chem.* **1984**, *88*, 3678. (c) Jones, G.; Malba, V. *Chem. Phys. Lett.* **1985**, *119*, 105.

(20) Usui, Y.; Misawa, H.; Sakuragi, H.; Tokumaru, K. *Bull. Chem. Soc. Jpn.* **1987**, *60*, 1573.

(21) Willner, I.; Eichen, Y.; Joselevich, E. *J. Phys. Chem.* **1990**, *94*, 3092.

(22) (a) Kisch, H.; Fernandez, A.; Wakatsuki, Y.; Yamazaki, H. *Z. Naturforsch.* **1985**, *40b*, 292. (b) Nakamura, K.; Kai, Y.; Yasuoka, N.; Kasai, N. *Bull. Chem. Soc. Jpn.* **1981**, *54*, 3300.

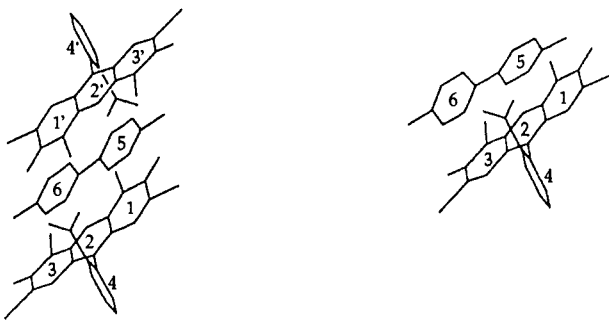
(23) (a) Poulos, A. T.; Kelley, C. K.; Simone, R. *J. Phys. Chem.* **1981**, *85*, 823. (b) Jones, G.; Malba, V. *Chem. Phys. Lett.* **1985**, *119*, 105. See ref 19c. (c) Hoffman, M. Z.; Prasad, D. R.; Jones, G., II; Malba, V. *J. Am. Chem. Soc.* **1983**, *105*, 6360. (d) Ebbesen, T. W.; Manring, L. E.; Peters, K. S. *J. Am. Chem. Soc.* **1984**, *106*, 7400. (e) Ebbesen, T. W.; Farraudi, G. *J. Phys. Chem.* **1983**, *87*, 3717. (f) Sullivan, B. P.; Dressick, W. J.; Meyer, T. J. *J. Phys. Chem.* **1982**, *86*, 1473. (g) Megehee, E. G.; Johnson, C. E.; Eisenberg, R. *Inorg. Chem.* **1989**, *28*, 2423.

(24) For a recent example of thermal charge transfer, see: Lehman, R. E.; Kochi, J. K. *J. Am. Chem. Soc.* **1991**, *113*, 501.

(25) All crystallographic computing was done on a CYBER 855 computer at the Hebrew University of Jerusalem, using a SHELX 1977 structure determination package.

Table II. Important Bond Lengths (Å) and Angles (deg)

[Eo <sup>2-</sup> -MV <sup>2+</sup> ]		[Eo <sup>2-</sup> -BV <sup>2+</sup> -Eo <sup>2-</sup> ; BV <sup>2+</sup> ]		[Phl <sup>2-</sup> -BV <sup>2+</sup> -Phl <sup>2-</sup> ; BV <sup>2+</sup> ]	
N1-C26	1.48 (2)	N1-C26	1.50 (3)	N1-C26	1.50 (1)
N2-C32	1.50 (2)	N2-C38	1.49 (2)	N2-C38	1.50 (1)
C23-C29	1.47 (2)	C21-C21'	1.48 (2)	C21-C21'	1.46 (1)
O1-C5	1.37 (1)	C33-C33'	1.54 (2)	C33-C33'	1.51 (1)
O1-C6	1.37 (1)	O1-C5	1.38 (1)	O1-C5	1.377 (8)
O2-C3	1.24 (1)	O1-C6	1.40 (2)	O1-C6	1.35 (1)
O3-C8	1.26 (1)	O2-C3	1.26 (2)	O2-C3	1.25 (1)
O4-C20	1.27 (1)	O3-C8	1.21 (2)	O3-C8	1.243 (9)
O5-C20	1.24 (1)	O4-C20	1.24 (2)	O4-C20	1.23 (1)
Br1-C2	1.90 (1)	O5-C20	1.25 (2)	O5-C20	1.23 (1)
Br2-C4	1.87 (1)	Br1-C2	1.93 (2)	Br1-C2	1.891 (7)
Br3-C7	1.88 (1)	Br2-C4	1.86 (1)	Br2-C4	1.884 (9)
Br4-C9	1.92 (1)	Br3-C7	1.87 (1)	Br3-C7	1.885 (8)
α(C11-C12-C14-C19)	73.46	Br4-C9	1.90 (1)	Br4-C9	1.891 (8)
α(C22-C23-C29-C30)	12.13	α(C11-C12-C14-C19)	70.7	C11-C16	1.731 (7)
		α(C22-C21-C21'-C22')	0.00	C12-C17	1.71 (1)
		α(C34-C33-C33''-C34')	0.00	C13-C18	1.717 (9)
				C14-C19	1.716 (7)
				α(C11-C12-C14-C19)	89.86
				α(C22-C21-C21'-C22')	0.00
				α(C34-C33-C33''-C34')	0.00

Table III. Interplanar Distances and Angles in Xanthene Dye-Bipyridinium<sup>a</sup> Complexes


structure	distance, Å (angle, deg)						
	d 1-5	d 2-5	d 2-6	d 3-6	d(N-N)-1 <sup>b</sup>	d(N-N)-2	d(N-N)-3
[Eo <sup>2-</sup> -MV <sup>2+</sup> ]	3.7 (2.39)	4.85 (1.69)	4.43 (13.45)	4.71 (16.33)	3.42	3.53	3.65
[Eo <sup>2-</sup> -BV <sup>2+</sup> -Eo <sup>2-</sup> ; BV <sup>2+</sup> ]	3.8 (4.85)	4.38 (5.66)	>6.0 (5.66)	5.88 (6.39)	3.30	3.50	3.70
[Phl <sup>2-</sup> -BV <sup>2+</sup> -Phl <sup>2-</sup> ; BV <sup>2+</sup> ]	3.8 (1.66)	3.87 (1.61)	5.33 (1.61)	4.45 (1.58)	3.41	3.47	3.45

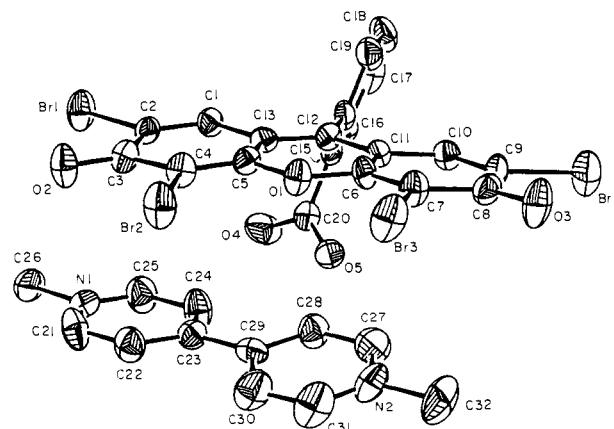
<sup>a</sup>Corresponding to intermolecular center-to-center ring distances and interplanar angles. <sup>b</sup>Distance of plumb line between center of ring and N-N bipyridinium line.

mizing the function  $\sum w(|F_o| - |F_c|)^2$ . A final difference Fourier synthesis map showed several peaks less than 1.0 e/Å<sup>3</sup>, 1.2 e/Å<sup>3</sup>, and 1.0 e/Å<sup>3</sup> (for [Eo<sup>2-</sup>-MV<sup>2+</sup>], [Eo<sup>2-</sup>-BV<sup>2+</sup>-Eo<sup>2-</sup>; BV<sup>2+</sup>], and [Phl<sup>2-</sup>-BV<sup>2+</sup>-Phl<sup>2-</sup>; BV<sup>2+</sup>] respectively) scattered about the unit cell without a significant feature. The discrepancy indicators,  $R = \sum ||F_o| - |F_c|| / \sum |F_o|$  and  $R_w = [\sum w(|F_o| - |F_c|)^2 / \sum w(|F_o|)^2]^{0.5}$ , are presented with other pertinent crystallographic data in Table I.

Single crystals of the complexes were obtained by slow evaporation of the solutions of the complexes. Single crystals of [Eo<sup>2-</sup>-MV<sup>2+</sup>] were obtained by mixing a solution of eosin in water with a solution of MV<sup>2+</sup> in water. Single crystals of [Eo<sup>2-</sup>-BV<sup>2+</sup>-Eo<sup>2-</sup>; BV<sup>2+</sup>] and [Phl<sup>2-</sup>-BV<sup>2+</sup>-Phl<sup>2-</sup>; BV<sup>2+</sup>] were obtained by mixing a 10% water in methanol solution (v/v) of the dyes: Eo<sup>2-</sup> or Phl<sup>2-</sup> with a 10% water in methanol BV<sup>2+</sup> solution followed by slow evaporation of the resulting solution. In all crystallization experiments, the bipyridinium salt was present in large excess relative to the xanthene dye. All resulting crystals were sealed in a capillary tube with a drop of the solvent.

## Results and Discussion

**Crystal Structure of Xanthene-Bipyridinium Complexes.** The crystal structure of the complex formed between eosin (1) and *N,N'*-dimethyl-4,4'-bipyridinium, methyl viologen, MV<sup>2+</sup> (2), is shown in Figure 1. Important angles and bond lengths in the complex are summarized in Table II. It is evident that the

Figure 1. X-ray structure of the [Eo<sup>2-</sup>-MV<sup>2+</sup>] complex.

intermolecular complex between eosin and MV<sup>2+</sup> generates a 1:1 complex, [Eo<sup>2-</sup>-MV<sup>2+</sup>]. The complex is surrounded by 13 molecules of water (not shown in Figure 1). The bipyridinium component neutralizes the negative charges of eosin in the unit

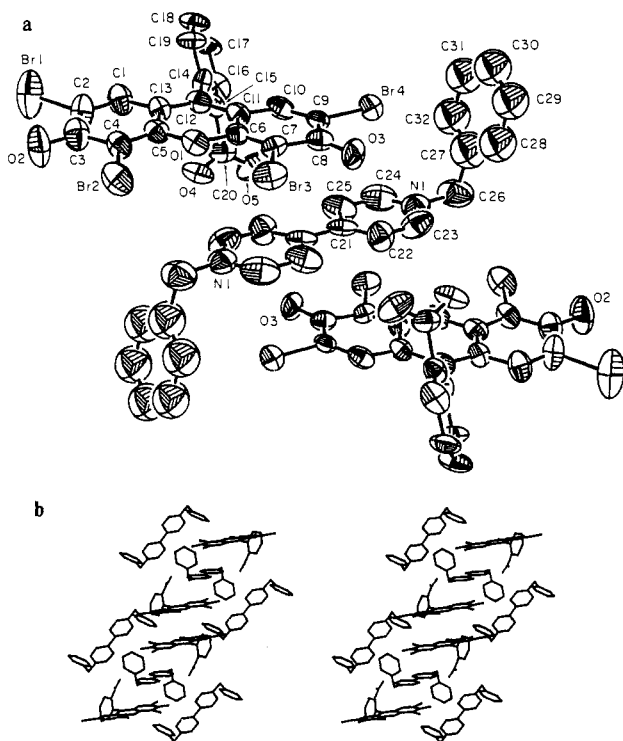


**Figure 2.** (a) X-ray structure of the  $[\text{Eo}^{2-}\text{-BV}^{2+}\text{-Eo}^{2-};\text{BV}^{2+}]$  complex. (b) Stacking of  $[\text{Eo}^{2-}\text{-BV}^{2+}\text{-Eo}^{2-};\text{BV}^{2+}]$  in the crystal, along the  $x$  axis.

cell. The dihedral angle between the two pyridinium rings is  $12.13^\circ$ . For comparison, in  $N,N'$ -dimethyl-4,4'-bipyridinium dichloride,  $\text{MV}^{2+}$ , the dihedral angle between the pyridinium rings<sup>26</sup> corresponds to  $0^\circ$ . Table III summarizes important interring distances and angles between eosin and  $\text{MV}^{2+}$  in the complex,  $[\text{Eo}^{2-}\text{-MV}^{2+}]$ . We see that one pyridinium ring is almost coplanar with rings numbered 1 and 2 of the eosin component. The center-to-center ring distance between these two units is 3.7 Å and reflects the existence of  $\pi$ -interactions between the two rings. This distance is in the range of values observed in other donor-acceptor complexes where  $\pi$ -interactions are operative.<sup>9,27</sup> The second pyridinium ring is deflected by an angle of  $16.33^\circ$  relative to ring 3 of eosin. The distance between these two rings is 4.71 Å, suggesting the absence of  $\pi$ -interactions between the rings.

A structurally different complex is formed between eosin and  $N,N'$ -dibenzyl-4,4'-bipyridinium,  $\text{BV}^{2+}$  (3) (Figure 2a). In this complex one bipyridinium component is intercalated between two eosin molecules, while the second bipyridinium component is remote from the  $\text{BV}^{2+}$ -eosin sandwich assembly and acts in charge neutralization of the structure. The overall composition of the eosin- $\text{BV}^{2+}$  complex is 2:1:1,  $[\text{Eo}^{2-}\text{-BV}^{2+}\text{-Eo}^{2-};\text{BV}^{2+}]$ . Table II provides important bond lengths and angles of the components included in the structure  $[\text{Eo}^{2-}\text{-BV}^{2+}\text{-Eo}^{2-};\text{BV}^{2+}]$ . It can be seen that in this complex the dihedral angle between the pyridinium rings is  $0^\circ$  in the bipyridinium unit encapsulated between the eosin components as well as in the free unit. The interring distances and angles in the complex  $[\text{Eo}^{2-}\text{-BV}^{2+}\text{-Eo}^{2-};\text{BV}^{2+}]$  are also included in Table III. It can be seen that the eosin-bipyridinium-eosin assembly is almost coplanar. The center-to-center distance between one bipyridinium ring (ring number 5) and ring number 1 of eosin is 3.81 Å. The distance between the second pyridinium ring (ring number 6) and the central ring of eosin (ring number 2) is 4.38 Å. The same distances are maintained between the intercalated bipyridinium unit and the complementary rings of the second eosin component. This eosin- $\text{BV}^{2+}$ -eosin assembly is symmetric in its structure and is characterized by an inversion center. The distances between the intercalated  $\text{BV}^{2+}$  and the two

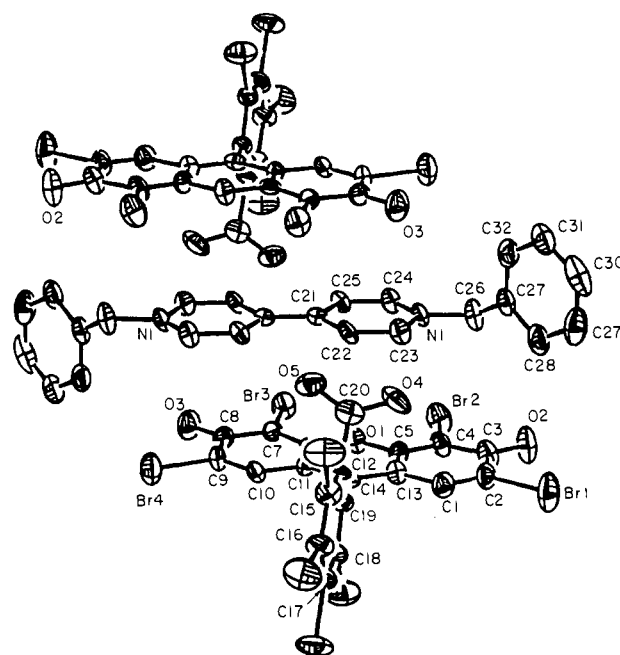
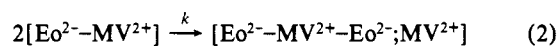
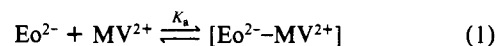


**Figure 3.** X-ray structure of the  $[\text{Phl}^{2-}\text{-BV}^{2+}\text{-Phl}^{2-};\text{BV}^{2+}]$  complex (the external  $\text{BV}^{2+}$  unit is omitted).

eosin components reveal that  $\pi$ -interactions are operative in the sandwich assembly.<sup>9,27</sup> The second  $\text{BV}^{2+}$  unit is remote from the sandwich structure and lacks intermolecular  $\pi$ -interactions.

Figure 2b shows the stacking of the complex  $[\text{Eo}^{2-}\text{-BV}^{2+}\text{-Eo}^{2-};\text{BV}^{2+}]$  along the  $x$  axis. It is evident that stacking of the eosin- $\text{BV}^{2+}$ -eosin assemblies takes place, resulting in  $\pi$ -interactions between adjacent eosin components of neighbor complexes. The interring distances between rings 1 and 3 and rings 2 and 2 of two neighboring eosin units are 3.92 and 3.93 Å, respectively. These values suggest that intercomplex as well as intracomplex  $\pi$ -interactions are operative in stabilizing the crystalline assembly  $[\text{Eo}^{2-}\text{-BV}^{2+}\text{-Eo}^{2-};\text{BV}^{2+}]$ . Aggregation of xanthene dyes in solutions are well-established and originate from intermolecular  $\pi$ -interactions.<sup>7</sup> The X-ray structure of the eosin- $\text{BV}^{2+}$  complex suggests that similar dye-dye interactions are present in the crystalline state. A very similar structure is obtained for the complex between phloxine,  $\text{Phl}^{2-}$  (4), and  $\text{BV}^{2+}$  (Figure 3). Here the structure  $[\text{Phl}^{2-}\text{-BV}^{2+}\text{-Phl}^{2-};\text{BV}^{2+}]$  is also formed. Yet, in this structure the intercomplex distances are  $>6$  Å. This can be attributed to the steric hindrance of the chloro-substituted phenyl groups on the dye backbone. Interestingly, the crystalline structure of the xanthene dye rose bengal,  $\text{Rb}^{2-}$ , and  $N,N'$ -dimethyl-4,4'-bipyridinium,  $\text{MV}^{2+}$ , reveals the presence of two intermolecular complexes in the unit cell.<sup>28</sup> The unit cell includes the 1:1 complex  $[\text{Rb}^{2-}\text{-MV}^{2+}]$  and the sandwich assembly,  $[\text{Rb}^{2-}\text{-MV}^{2+}\text{-Rb}^{2-};\text{MV}^{2+}]$ .

**Eosin-Methyl Viologen Complexes in Solution.** The formation of eosin-methyl viologen complexes can be followed in solutions. We observe the primary formation of the eosin-methyl viologen monomer complex,  $[\text{Eo}^{2-}\text{-MV}^{2+}]$  (eq 1), and its subsequent transformation into the eosin-methyl viologen sandwich assembly,  $[\text{Eo}^{2-}\text{-MV}^{2+}\text{-Eo}^{2-};\text{MV}^{2+}]$  (eq 2). Figure 4 shows the spectral



changes occurring upon addition of  $\text{MV}^{2+}$  to a DMF solution of eosin. Initially, the absorption band of eosin is red-shifted, and a species with an absorption maximum at  $\lambda = 532$  nm is formed (the absorption band of disodium eosin is at  $\lambda_{\text{max}} = 528$  nm). The

(26) Russell, J. H.; Wallwork, S. C. *Acta Crystallogr.* **1972**, *B28*, 1527.  
(27) In ref 4a, chapters 2 and 8.

(28) Willner, I.; Eichen, Y.; Joselevich, E. Unpublished results.

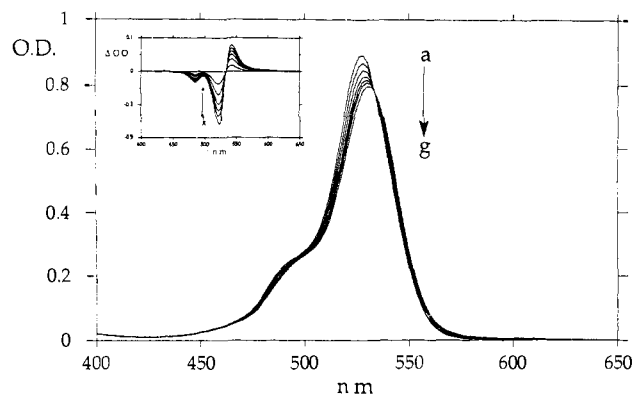


**Figure 4.** Absorption spectra and differential absorption spectra (inserted graph) of eosin,  $1 \times 10^{-5}$  M in DMF, in the presence of methyl viologen,  $MV^{2+}$ , at the following concentrations: (a) 0 M, (b)  $8 \times 10^{-6}$  M, (c)  $1.6 \times 10^{-5}$  M, (d)  $2.4 \times 10^{-5}$  M, (e)  $3.2 \times 10^{-5}$  M, (f)  $8.6 \times 10^{-5}$  M, (g)  $9.6 \times 10^{-5}$  M.

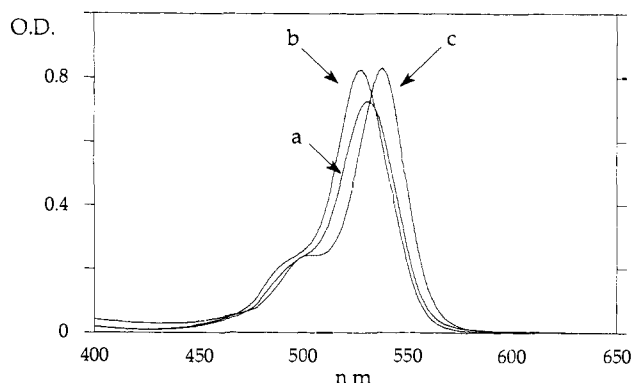


**Figure 5.** Absorption spectra of eosin,  $1 \times 10^{-5}$  M in DMF, in the forms: (a) disodium salt, (b)  $[Eo^{2-}-MV^{2+}]$ , (c)  $[Eo^{2-}-BV^{2+}-Eo^{2-};BV^{2+}]$ .

presence of an isosbestic point within the consecutive additions of  $MV^{2+}$  implies that a pure and single species is formed. This primary complex ( $\lambda_{max} = 532$  nm) is attributed to a monomer complex structure of eosin- $MV^{2+}$  (eq 1; vide infra). From the changes in the absorption spectrum of eosin at different concentrations of  $MV^{2+}$  and using the Benesi-Hildebrand relation,<sup>29</sup> the association constant,  $K_a$ , of the monomer structure is determined. The calculated value of  $K_a$  is  $91\,000 \pm 910$  M<sup>-1</sup>, corresponding to a free energy change of  $\Delta G^\circ = -6.74$  kcal mol<sup>-1</sup> (at 298 K) associated with the formation of the complex.

The primary intermolecular structure of the complex  $[Eo^{2-}-MV^{2+}]$  is unstable in the DMF solution and is transformed into a secondary product, which is red-shifted by 6 nm as compared to the monomer complex (Figure 5). The interconversion rate is temperature-dependent, and as the temperature is elevated the rate of the interconversion is enhanced. The secondary product formed is attributed to the intermolecular sandwich assembly,  $[Eo^{2-}-MV^{2+}-Eo^{2-};MV^{2+}]$ . From the changes in the absorption bands associated with the conversion of the monomer to the sandwich assembly (Figure 6) (decrease of the band at  $\lambda = 532$  nm ( $\epsilon = 72\,600$  M<sup>-1</sup> cm<sup>-1</sup>) and increase of the band at  $\lambda = 538$  nm ( $\epsilon = 82\,600$  M<sup>-1</sup> cm<sup>-1</sup>), the rate constant<sup>30</sup> for the interconversion of the complex structure is determined by eq 2 to be  $k = 57.3$  M<sup>-1</sup> s<sup>-1</sup> at 331 K. The temperature dependence of the rate constant gives a linear Arrhenius plot. The activation energy associated with the conversion of the monomer complex to the intermolecular sandwich assembly corresponds to  $E_a = 25.3 \pm 0.5$  kcal mol<sup>-1</sup>.

In dimethyl sulfoxide (DMSO), similar qualitative behavior for the formation of the complexes is observed. Yet, in this solvent, the monomer structure exhibits higher stability, and intercon-

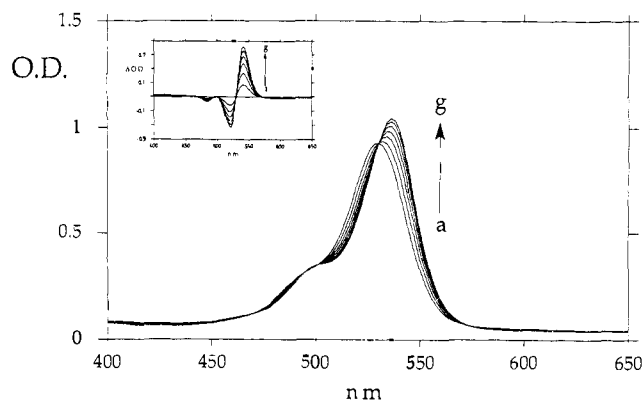


**Figure 6.** Absorption spectra and differential absorption spectra (inserted graph) of the eosin-methyl viologen complex,  $1 \times 10^{-5}$  M in DMF, at 331 K as a function of time: (a)  $t = 0$  min, (b)  $t = 2$  min, (c)  $t = 4$  min, (d)  $t = 6$  min, (e)  $t = 8$  min, (f)  $t = 10$  min, (g)  $t = 12$  min.

version to the dimer complex is observed after several weeks at room temperature.

Insight into the structures of the eosin-methyl viologen assemblies in solutions is obtained by NMR analyses. Figure 7 shows the NMR spectra of the eosin-methyl viologen complexes in DMSO and DMF solvents. It has been suggested that, in DMSO (Figure 7a), the resulting eosin- $MV^{2+}$  complex is in a monomer structure and interconversion to the dimer structure is very slow. Indeed, the <sup>1</sup>H NMR spectrum is consistent with a monomer structure of the complex. We observe a single AA'BB' spectrum for the  $MV^{2+}$  protons at  $\delta_{Ha}$  9.12 and  $\delta_{Hb}$  8.82 ppm and a singlet for the *N*-methylpyridinium protons at  $\delta$  4.37 ppm. The bands at  $\delta$  7.98, 7.53, 7.45, 7.09, and 7.02 ppm correspond to protons H<sub>1</sub>, H<sub>2</sub>, H<sub>3</sub>, H<sub>4</sub>, and H<sub>5</sub> of eosin, respectively. The integration ratio between the viologen protons and eosin protons reflects a molar ratio of 1:1, consistent with an intermolecular monomer complex structure,  $[Eo^{2-}-MV^{2+}]$ . It should be noted that broadening of the  $MV^{2+}$  bands is observed. This originates from thermal charge transfer occurring in the complex assembly, as will be discussed later. In DMF the spectrum displayed in Figure 7b corresponds to the intermolecular sandwich assembly,  $[Eo^{2-}-MV^{2+}-Eo^{2-};MV^{2+}]$ . In fact, to solubilize the solid complex in DMF, heating of the sample is required. Immediately after the components are dissolved, the <sup>1</sup>H NMR spectrum of the resulting solution includes, in addition to the spectrum shown in Figure 7b, the characteristic bands of the monomer complex, as discussed for the DMSO solution. Within a few minutes, the monomer bands disappear and the spectrum of a pure complex (Figure 7b) corresponding to the dimer structure is obtained. These results are consistent with the previously discussed interconversion of the monomer complex to the intercalated complex structure in DMF solution. Analysis of the <sup>1</sup>H NMR spectrum reflects the formation of the sandwich assembly,  $[Eo^{2-}-MV^{2+}-Eo^{2-};MV^{2+}]$ . We realize that the spectrum includes two AA'BB' patterns corresponding to two distinct and different  $MV^{2+}$  components.<sup>31</sup> One AA'BB' pattern at  $\delta_{Ha}$  9.35 and  $\delta_{Hb}$  8.40 ( $J_{AB} = 6.8$  Hz) corresponds to one  $MV^{2+}$  unit, and the second AA'BB' pattern,  $\delta_{Hc}$  8.89 and  $\delta_{Hd}$  8.08 ppm ( $J_{CD} = 6.4$  Hz) belongs to the second  $MV^{2+}$  component. The bands at  $\delta$  8.25, 7.84, 7.78, 7.57, and 7.07 ppm correspond to protons H<sub>1</sub>, H<sub>2</sub>, H<sub>3</sub>, H<sub>4</sub>, and H<sub>5</sub> of the eosin unit, respectively. The integration ratio of the eosin protons and each AB spectrum corresponds to 2:1:1, respectively, implying that two different bipyridinium components form an intermolecular complex with two eosin units, which are

(31) The four  $MV^{2+}$  multiplets are divided into two pairs, each pair corresponding to a different  $MV^{2+}$  component on the basis of TOCSY experiment that shows only through-bond correlations. The absence of through-space correlations (NOE and ROE) in NOESY and ROESY spectra between one pair and the other confirms that only two multiplets correlate to each  $MV^{2+}$  component. A configuration where the two  $MV^{2+}$  are equivalent but each bipyridinium ring is present in a different environment can be excluded. Such a complex configuration would yield four multiplets exhibiting a through-space correlation between the H<sub>1</sub> multiplets.

(29) Benesi, H. A.; Hildebrand, J. H. *J. Am. Chem. Soc.* **1949**, *71*, 2703.

(30) A bimolecular process is assumed in the kinetic analysis.

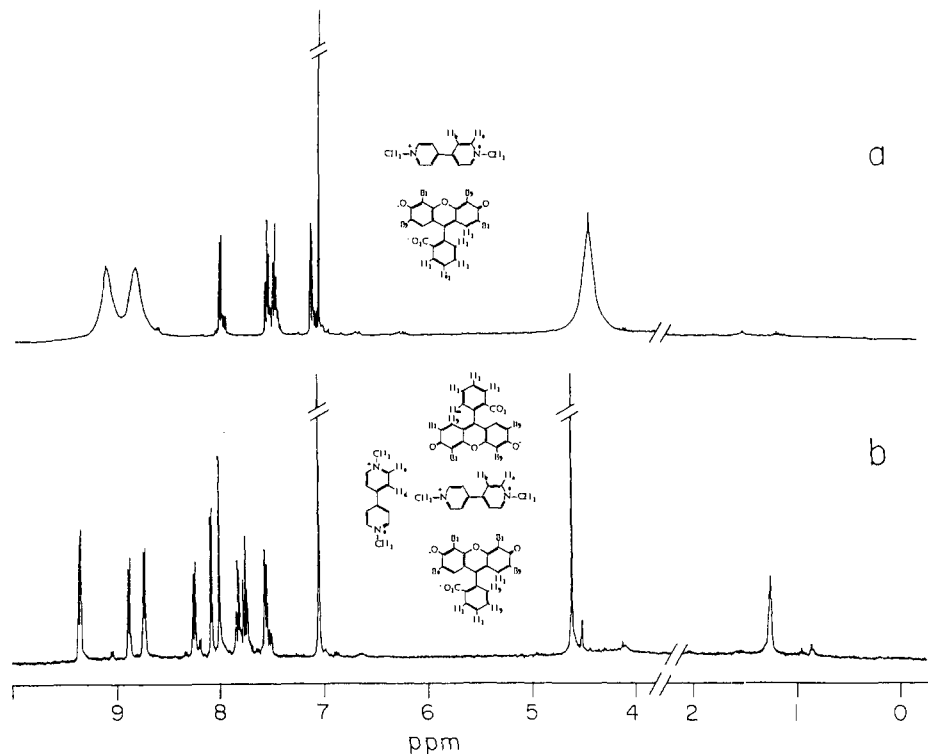
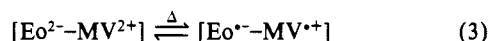


Figure 7.  $^1\text{H}$  NMR spectra (295 K) of the complex between eosin and methyl viologen (a) in  $\text{DMSO-}d_6$  and (b) in  $\text{DMF-}d_7$ .

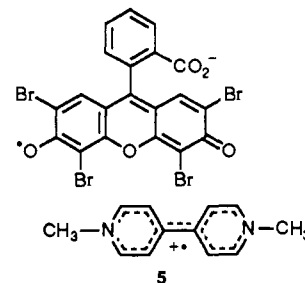
equivalent in the supramolecular structure. The equivalency of the two eosin units suggests that a symmetric intermolecular structure of these components relative to the bipyridinium units exists. Furthermore, the bipyridinium methyl substituents of the two  $\text{MV}^{2+}$  units present in the complex differ substantially. The methyl groups of one bipyridinium unit appear at  $\delta_{\text{CH}_3}$  4.64 ppm, close to the value observed for free  $\text{MV}^{2+}$  in DMF. Thus, this bipyridinium unit is probably located in an external position in the intermolecular complex, exhibiting the character of free  $\text{MV}^{2+}$ . The methyl groups of the second  $\text{MV}^{2+}$  unit are substantially high field shifted,  $\delta_{\text{CH}_3}$  1.26 ppm. The high field shift of these protons is attributed to the location of the methyl substituents in the paramagnetic ring current region of the eosin units. Thus, one  $\text{MV}^{2+}$  component is probably intercalated between two eosin units, while the second  $\text{MV}^{2+}$  component is in an external position in the resulting intermolecular complex. Although we were unable to determine distances between the components in the intermolecular assembly,<sup>31</sup> its symmetry properties suggest that a structure closely related to that in the crystalline state,  $[\text{Eo}^{2-};\text{MV}^{2+};\text{Eo}^{2-};\text{MV}^{2+}]$ , is also present in solution. The  $^1\text{H}$  NMR spectrum of the complex in DMSO solution after 2 weeks is similar to the spectrum for the sandwich complex  $[\text{Eo}^{2-};\text{MV}^{2+};\text{Eo}^{2-};\text{MV}^{2+}]$  in DMF. Thus, slow interconversion of the monomer complex,  $[\text{Eo}^{2-};\text{MV}^{2+}]$ , to the sandwich structure occurs in DMSO.

**Charge Transfer in Eosin–Methyl Viologen Complexes.** The  $^1\text{H}$  NMR spectrum of the monomer complex of eosin– $\text{MV}^{2+}$  in DMSO is shown in Figure 7a. It is evident that the bands of the  $\text{MV}^{2+}$  monomer in DMSO (where the monomer structure is moderately stable) are strongly temperature dependent (Figure 8). As the sample is heated, the characteristic bands of the  $\text{MV}^{2+}$  component are broadened, and at 320 K the bands entirely disappear. This change is reversible and, upon cooling, the original spectrum is recorded. Broadening of the spectrum at room temperature and disappearance of the  $\text{MV}^{2+}$  bands at higher temperatures is attributed to thermal population of the charge-transfer level (eq 3), i.e., in this complex, the charge-transfer level is sufficiently close to the ground state to allow thermal charge transfer to occur. Upon heating the sample, the charge-transfer



level is further populated, and hence the broadening effect is

substantiated. It should be noted that only a fraction of the complex is in charge-transfer state (vide infra), and thus only broadening of the  $^1\text{H}$  NMR bands, rather than complete scavenging of the signals, is observed. Furthermore, broadening of the NMR bands is observed for the  $\text{MV}^{2+}$  component, but almost no effect on the bands of eosin is detected. This is attributed to the delocalization vs localization of the radicals in the two units of the complex (5). The resulting radical cation is delocalized over the molecular backbone, leading to broadening of its NMR bands. On the other hand, the radical on the eosin component is localized, and consequently its NMR bands are unaffected.



Thermal population of the charge-transfer level in the  $[\text{Eo}^{2-};\text{MV}^{2+}]$  monomer complex is further supported by ESR and absorption spectroscopy measurements. The DMSO solution that exhibits the NMR spectrum shown in Figure 8a gives an ESR spectrum, shown in Figure 9. The fact that the ESR spectrum consists of absorption and emission bands implies that the spectrum originates from two radicals. In fact, the spectrum consists of  $\text{MV}^{\bullet+}$  and  $\text{Eo}^{\bullet-}$ . Thus, the solution of the monomer complex,  $[\text{Eo}^{2-};\text{MV}^{2+}]$  includes the charge-transfer species 5, formed through thermal population of the charge-transfer state (eq 3). In DMF solution where the monomer complex  $[\text{Eo}^{2-};\text{MV}^{2+}]$  is initially formed, a similar ESR spectrum is observed. Nevertheless, the ESR spectrum decays with the concomitant formation of the dimer complex,  $[\text{Eo}^{2-};\text{MV}^{2+};\text{Eo}^{2-};\text{MV}^{2+}]$ , where no thermal population of the charge-transfer state is observed.

The extent of thermal population of the charge-transfer level is determined by the charge-transfer energy gap and depends on the temperature of the medium. Although the presence of thermal charge-transfer products  $[\text{Eo}^{\bullet-};\text{MV}^{\bullet+}]$  in the DMSO solution is

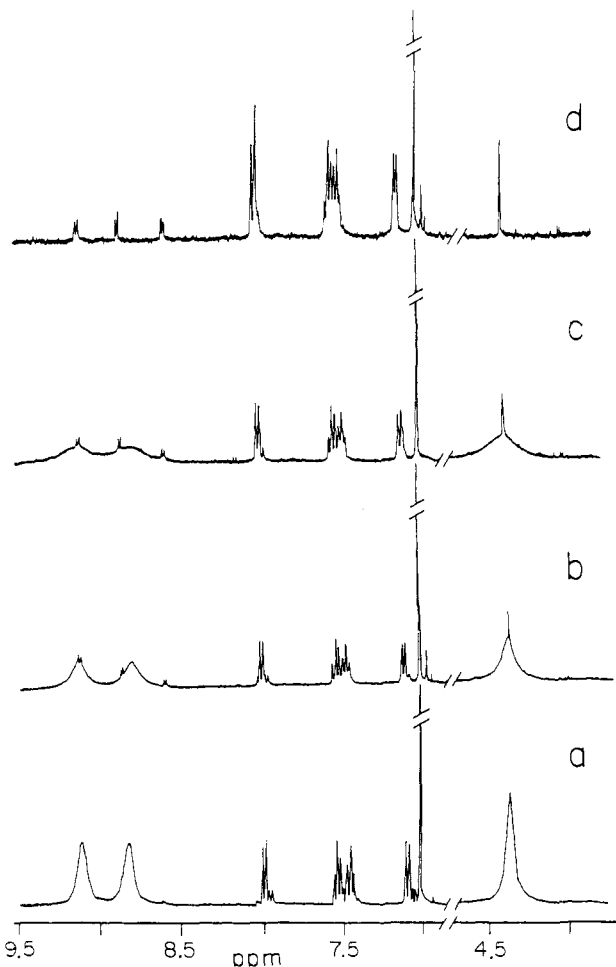


Figure 8. Temperature dependence of the  $^1\text{H}$  NMR spectrum of  $[\text{Eo}^{2-}\text{-MV}^{2+}]$  in  $\text{DMSO-}d_6$ : (a) 290 K, (b) 300 K, (c) 310 K, (d) 320 K.

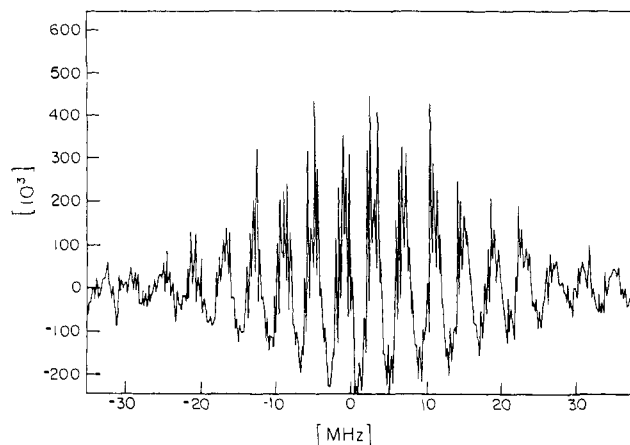


Figure 9. ESR spectrum of the  $[\text{Eo}^{2-}\text{-MV}^{2+}]$  complex in DMSO at 295 K.

evident from ESR measurements, their identification by absorption spectroscopy is impossible due to their low concentration. In turn, the primary monomer complex,  $[\text{Eo}^{2-}\text{-MV}^{2+}]$ , formed in DMF solution allows the spectroscopic identification of the thermal charge-transfer population. Figure 10 shows the absorption spectrum of the monomer complex,  $[\text{Eo}^{2-}\text{-MV}^{2+}]$ , immediately after generation in the DMF solution at 340 and 331 K. It is evident that the characteristic absorption band of  $\text{MV}^{+}$  is observable at  $\lambda = 396$  nm. The amount of  $\text{MV}^{+}$  detectable in the spectra is temperature-dependent and, as the temperature is lowered, its concentration is decreased. The population of the

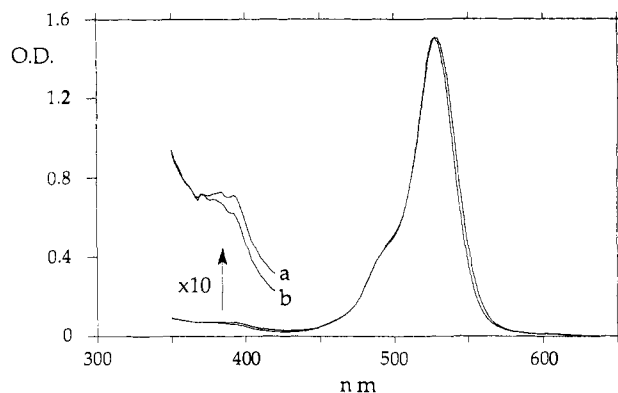


Figure 10. Absorption spectra of the  $[\text{Eo}^{2-}\text{-MV}^{2+}]$  complex in DMF: (a) 340 K and (b) 331 K.

charge-transfer state as a function of temperature is given by eq 4, where  $n_1/n_2$  is the population ratio of the charge-transfer and ground-state levels and  $\Delta E$  is the charge-transfer energy gap.

$$n_1/n_2 = e^{-\Delta E/RT} \quad (4)$$

From the absorption band of  $\text{MV}^{+}$  ( $\lambda = 396$  nm ( $\epsilon = 36\,500$   $\text{M}^{-1}\text{cm}^{-1}$ )) at 340 K, we estimate that in DMF solution ca. 2.5% of the complex is in the thermally excited charge-transfer state (eq 3). Thus, the HOMO-LUMO charge-transfer energy gap in the complex is estimated to be  $870$   $\text{cm}^{-1}$ . The fact that the charge-transfer state of the complex is nondetectable by absorption spectroscopy in DMSO suggests that the energy gap in this solvent is higher, and thus the thermal population of the LUMO state is substantially lower.

## Conclusions

Xanthene dye and  $N,N'$ -dialkyl-4,4'-bipyridinium form intermolecular assemblies in the solid state and solution phase. The dye eosin,  $\text{Eo}^{2-}$ , and  $N,N'$ -dimethyl-4,4'-bipyridinium,  $\text{MV}^{2+}$ , in the crystalline state form a 1:1 complex assembly stabilized by electrostatic and  $\pi$ -interactions. With  $N,N'$ -dibenzyl-4,4'-bipyridinium,  $\text{BV}^{2+}$ , the dye eosin forms a crystalline complex where one bipyridinium component is intercalated between two  $\text{Eo}^{2-}$  units and stabilized by electrostatic and  $\pi$ -interactions, while the second  $\text{BV}^{2+}$  is located in an external position to the complex structure and acts in charge neutralization,  $[\text{Eo}^{2-}\text{-BV}^{2+}\text{-Eo;BV}^{2+}]$ . The dye phloxine,  $\text{Phl}^{2-}$ , forms a complex with  $\text{BV}^{2+}$  that is structurally very similar to that formed by  $\text{Eo}^{2-}$ .

In solution (DMF and DMSO),  $\text{Eo}^{2-}$  and  $\text{MV}^{2+}$  form, as an initial product, the kinetically favored 1:1 complex,  $[\text{Eo}^{2-}\text{-MV}^{2+}]$ . The latter complex rearranges to a thermodynamically stable complex assembly that includes two different bipyridinium units associated with two equivalent  $\text{Eo}^{2-}$  units.  $^1\text{H}$  NMR studies suggest that the thermodynamically stable complex includes a sandwich structure where one  $\text{MV}^{2+}$  unit is symmetrically trapped between two  $\text{Eo}^{2-}$  components, while the second  $\text{MV}^{2+}$  unit is externally positioned to the complex assembly,  $[\text{Eo}^{2-}\text{-MV}^{2+}\text{-Eo}^{2-};\text{MV}^{2+}]$ . In DMF solution, the transformation of  $[\text{Eo}^{2-}\text{-MV}^{2+}]$  to  $[\text{Eo}^{2-}\text{-MV}^{2+}\text{-Eo}^{2-};\text{MV}^{2+}]$  proceeds with a bimolecular rate constant corresponding to  $k = 57.3$   $\text{M}^{-1}\text{s}^{-1}$  (at 331 K) and  $E_a = 25.3 \pm 0.5$   $\text{kcal mol}^{-1}$ . NMR, ESR, and spectroscopic analyses reveal that the monomer complex  $[\text{Eo}^{2-}\text{-MV}^{2+}]$  exhibits thermal population of the charge-transfer level, and ca. 2.5% of the complex (in DMF solution) exists in the charge-transfer state,  $[\text{Eo}^{+}\text{-MV}^{+}]$  at 340 K.

The stable and different structures of eosin and bipyridinium components suggest that electrostatic, charge-transfer, and  $\pi$ -interactions play important roles in the stabilization of these assemblies. Further experiments to design other bipyridinium-xanthene dye complexes and to examine the conductivities of these organic donor-acceptor assemblies are under way in our laboratory.

**Acknowledgment.** The support of the project by the U.S.-Israel

Binational Fund is gratefully acknowledged. Y.E. acknowledges the support of the Ben Gurion Fellowship Fund. The use of the Margaret Thatcher Research Center facilities (NMR, ESR, and Laser instruments) is gratefully acknowledged. We thank Mr. G. Zilber for experimental assistance.

Registry No. 1·2·13H<sub>2</sub>O, 137122-82-8; 91·3·2H<sub>2</sub>O, 137122-84-0; 3·

4·3CH<sub>3</sub>OH, 137143-71-6.

**Supplementary Material Available:** Tables of thermal parameters, bond lengths and bond angles, and calculated positional parameters and estimated standard deviations for the different complexes (22 pages). Ordering information is given on any current masthead page.

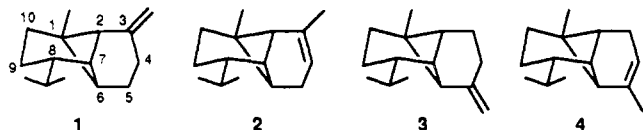
## Total Syntheses of (±)-α- and (±)-β-Copaene and Formal Total Syntheses of (±)-Sativene, (±)-*cis*-Sativenediol, and (±)-Helminthosporal†

Ernest Wenkert,\* Brett C. Bookser, and Thomas S. Arrhenius

Contribution from the Department of Chemistry (0506), University of California—San Diego, La Jolla, California 92093. Received April 29, 1991

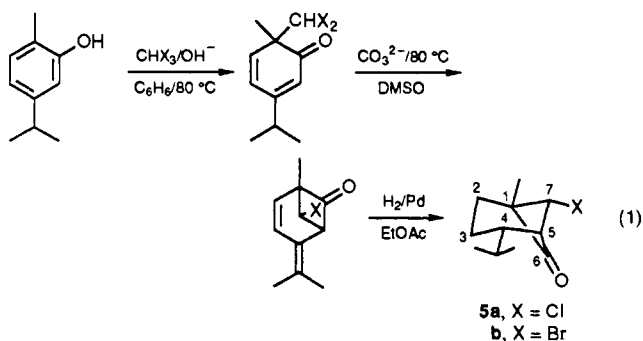
**Abstract:** Conversion of the previously reported, carvacrol-based 4(*S*<sup>\*</sup>)-isopropyl-7(*R*<sup>\*</sup>)-chlorobicyclo[3.1.1]heptan-6-one and its bromo equivalent into (±)-α- and (±)-β-copaene is described. Model 5-nor-β-copaene was synthesized in the following manner: (a) γ-(trimethylsilyl)propargyllithium addition, (b) tri-*n*-butylstannane-induced, dehalogenative, free-radical cyclization and either fluoride-promoted or *p*-toluenesulfonic acid-catalyzed desilylation in the proper sequence, and (c) free-radical deoxygenation of the resultant tricyclic alcohol via a thioester. The β-copaene synthesis followed a similar procedure except for the addition of the lithio derivative of δ-(trimethylsilyl)homopropargyl *p*-tolyl sulfone in step a, sodium amalgam reduction of the intermediate sulfones either before or following step b, and alcohol deoxygenation by photolysis of an acetate in step c. Treatment of (±)-β-copaene with hydrogen iodide caused isomerization into (±)-α-copaene. Variation of the β-copaene synthesis scheme permitted a tie-up with sativene. Thus, ozonolysis of the 6-hydroxy-5-(*p*-tolylsulfonyl)-β-copaene intermediate followed by base-induced sulfinate elimination, acid- or base-catalyzed skeletal rearrangement, monothioacetal formation, and desulfurization yielded a ketone, whose one-step transformation into (±)-sativene has been reported earlier. Finally, borohydride reduction of the sulfinate elimination product, acid-promoted skeletal rearrangement, and methylolithium addition led to an alcohol, whose conversion into (±)-*cis*-sativenediol and (±)-helminthosporal has been recorded earlier.

β-Copaene (1), α-copaene (2), β-ylangene (3), and α-ylangene (4) are tricyclic sesquiterpenes, whose unusual ring skeletons make them challenging goals of total synthesis. Early constructions



of two or more of these natural products depended on intramolecular displacements within *cis*-decalin frames<sup>1,2</sup> or on an intramolecular ene-ketene cyclization<sup>3</sup> for the formation of the central four-membered ring and also depended on the isopropyl group being attached to its cyclohexane nucleus at a late stage of the reaction sequences.<sup>1-3</sup> The absence of stereochemical control in the introduction of the three-carbon side chain in two of the three syntheses<sup>2,3</sup> and low control in one approach of the third synthesis<sup>1</sup> led to copaene-ylangene pairs as the final products. For this reason it was of interest to develop yet another route of synthesis, whose aim would be the formation of a unique sesquiterpene, e.g., β-copaene (1).

The new synthesis was predicated on early construction of the cyclobutane and isopropylated cyclohexane nuclei in configurationally correct forms, possessing properly placed functional groups for elaboration of the olefinic six-membered ring. This task has been accomplished some time ago in the four-step buildup of ketones **5** via Reimer-Tiemann chemistry on carvacrol (eq 1).<sup>4,5</sup> The remaining endeavor required the utilization of the halo and carbonyl groups of the ketones for the introduction of the third,



stereochemically inconsequential ring. It was hoped that a reaction sequence would be initiated by addition of an acetylene-bearing chain to the carbonyl function, fashioning a free-radical cyclization<sup>6</sup> in the direction of the β-copaene system by reductive

(1) Heathcock, C. H.; Badger, R. A.; Patterson, J. W., Jr. *J. Am. Chem. Soc.* 1967, 89, 4133.

(2) Corey, E. J.; Watt, D. S. *J. Am. Chem. Soc.* 1973, 95, 2303.

(3) Snider, B. B.; Kulkarni, Y. S.; Niwa, M.; Ron, E. *J. Org. Chem.* 1987, 52, 1568.

(4) Wenkert, E.; Bakuzis, P.; Baumgarten, R. J.; Doddrell, D.; Jeffs, P. W.; Leicht, C. L.; Mueller, R. A.; Yoshikoshi, A. *J. Am. Chem. Soc.* 1970, 92, 1617.

(5) Wenkert, E.; Arrhenius, T. S.; Bookser, B.; Guo, M.; Mancini, P. *J. Org. Chem.* 1990, 55, 1185.

(6) (a) Glese, B. *Radicals in Organic Synthesis; Formation of Carbon-Carbon Bonds*; Pergamon Press: Oxford, 1986. (b) Neumann, W. P. *Synthesis* 1987, 655. (c) Ramaiah, M. *Tetrahedron* 1987, 43, 3541. (d) Curran, D. P. *Synthesis* 1988, 417, 489. (e) Thebtaranonth, C.; Thebtaranonth, Y. *Tetrahedron* 1990, 46, 1385.

† Presented as an invited lecture at the 17th International Symposium on the Chemistry of Natural Products, New Delhi, India, February 4-9, 1990.